

High quality tensile-strained *n*-doped germanium thin films grown on InGaAs buffer layers by metal-organic chemical vapor deposition

R. Jakomin,^{1,a)} M. de Kersauson,² M. El Kurdi,^{2,b)} L. Largeau,¹ O. Mauguin,¹ G. Beaudoin,¹ S. Sauvage,² R. Ossikovski,³ G. Ndong,³ M. Chaigneau,³ I. Sagnes,¹ and P. Boucaud^{2,c)}

¹Laboratoire de Photonique et de Nanostructures, CNRS-UPR 20, Route de Nozay, 91460 Marcoussis, France

²Institut d'Electronique Fondamentale, CNRS-Univ. Paris-Sud II, Bâtiment 220, 91405 Orsay, France

³LPICM, Ecole Polytechnique, CNRS, 91128 Palaiseau Cedex, France

(Received 20 December 2010; accepted 4 February 2011; published online 28 February 2011)

We show that high quality tensile-strained *n*-doped germanium films can be obtained on InGaAs buffer layers using metal-organic chemical vapor deposition with isobutyl germane as germanium precursor. A tensile strain up to 0.5% is achieved, simultaneously measured by x-ray diffraction and Raman spectroscopy. The effect of tensile strain on band gap energy is directly observed by room temperature direct band gap photoluminescence. © 2011 American Institute of Physics.

[doi:10.1063/1.3559231]

Laser emission has recently been demonstrated under optical pumping at room temperature using germanium, an indirect band gap material, as the active layer.¹ This result sets a new paradigm for silicon photonics as efficient optical sources made of group IV materials have long been considered as a dead end. Two main features can explain that a net optical gain has been obtained with germanium. The first one is the application of a tensile strain which lowers the energy difference between the indirect *L* valley and the zone center Γ valley. Meanwhile, the tensile strain lifts the degeneracy between heavy hole and light hole valence bands. Consequently, strong optical gain has been theoretically predicted for tensile-strained materials using either effective-mass approaches^{2–5} or a 30 band $\mathbf{k}\cdot\mathbf{p}$ formalism.⁶ The second feature is associated with the *n*-type doping of the germanium which leads to a more efficient population of the zone center Γ valley and an enhanced optical recombination at Brillouin zone center.^{7,8} The direct growth of germanium on silicon substrate leads to a tensile strain around 0.25%.⁹ However, the optical gain is expected to be larger as the tensile strain is increased, a direct band gap material being even predicted for a tensile strain around 2%.¹⁰ Several approaches have thus been investigated to apply a significant strain on germanium, larger than the one resulting from the difference of thermal expansion coefficients between germanium and silicon. The growth on GeSn buffer layers has been considered by Menendez and co-workers.^{11,12} Mechanical deformation of Ge films has been shown to be an effective method to tailor *ex situ* the properties of germanium membranes or microresonators.^{4,13,14} A third option is to grow the germanium films on III–V buffer layers with a lattice constant larger than the one of germanium. This approach has been first demonstrated by Bai *et al.*¹⁵ by growing germanium on relaxed InGaAs buffer layers. Even if the growth of Ge on InGaAs requires a III–V material, i.e., not an approach using only group IV elements, it exhibits several advantages.

Strong tensile strains, larger than 0.25%, can be obtained by this technique thus leading potentially to enhanced optical recombination properties and lower thresholds for lasers. The growth on template layers can also be considered as an intermediate processing step before bonding as it is done to obtain tensile-strained silicon layer on insulator through the growth on GeSi buffer layers.

In this letter, we show that tensile-strained *n*-doped Ge layers with high optical quality can be obtained by growth on InGaAs buffer layers. The samples were grown on GaAs substrates by metal-organic chemical vapor deposition. One crucial aspect resides in the growth of germanium in a III–V reactor since the Ge/InGaAs/GaAs structure involves both III–V and group IV elements. For this, a suitable metal-organic precursor is necessary. Ge growth is obtained by using the novel isobutyl germane (IBGe) source, developed by Rohm and Haas.^{16,17} IBGe is a liquid metal-organic precursor safer than GeH₄ and compatible with the III–V gas exhaust system. Ge and InGaAs growth is performed in a low pressure (70 Torr) metal-organic vapor phase epitaxy system (VEECO D180) by using hydrogen (H₂) as carrier gas. Trimethyl-indium, trimethyl-gallium, and arsine (AsH₃) are used as In, Ga, and As precursors. InGaAs templates of around 1 μm thickness, with different In contents were grown on GaAs(100) substrate at 650 °C. The InGaAs templates are expected to be plastically relaxed on GaAs substrate and free of extended defects. An AsH₃ flow is maintained before the Ge growth to prevent As desorption from the template. The growth temperature is 650 °C and the bubbler conditions for IBGe are 5 °C, 600 Torr, and 100 SCCM (SCCM denotes standard cubic centimeter per minute at STP) flow. An AsH₃ flow is also supplied during Ge growth to realize high *n*-doped layers. In these conditions a free electron density of $2.2 \times 10^{19} \text{ cm}^{-3}$, at room temperature, is measured.

The structure of the 50 nm thick Ge layer deposited on the In-richest InGaAs buffer was investigated using a JEOL 2200 FS transmission electron microscope (TEM)/scanning TEM (STEM) equipped with a Cs-probe aberration corrector. Figure 1(a) shows a conventional TEM image of the

^{a)}Electronic mail: roberto.jakomin@lpn.cnrs.fr.

^{b)}Electronic mail: moustafa.el-kurdi@ief.u-psud.fr.

^{c)}Electronic mail: philippe.boucaud@ief.u-psud.fr.

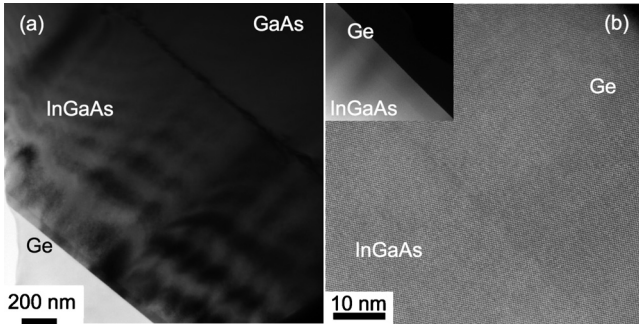


FIG. 1. (a) Conventional cross-sectional TEM observation of the sample with 9.8% In-rich buffer layer and (b) HAADF images of the interface between the InGaAs and Ge layers.

whole structure. The InGaAs layer appears free of extended defects. The dislocations accommodating the lattice mismatch are well located at the interface between the InGaAs buffer layer and the GaAs substrate. No threading dislocations in the Ge/InGaAs layers are observed over wider zones. Figure 1(b) shows Z-contrast high angle annular dark field (HAADF) images collected in the STEM mode. In the low magnification image (inset), due to their relative Z numbers, the Ge layer appears with a darker contrast than the InGaAs layer. The high magnification image shows the very good lattice continuity at the Ge/InGaAs interface. The InGaAs thickness is 1.21 μm , while the Ge layer is 47.5 nm thick, in agreement with the expected values.

The composition and strain of InGaAs and Ge were determined by high resolution XRD reciprocal space mapping (HRXRD-RSM) collected with a Rigaku smartlab diffractometer equipped with a rotating anode. 004, 224, and $-2-24$ RSMs were collected along the four $\langle 110 \rangle$ azimuthal directions. Multidirectional space mappings allow to eliminate the effect of potential lattice misorientations. Figure 2 shows RSMs collected along the same azimuthal direction around the (004) diffraction area (a) and around the 224 diffraction area (b) on the 50 nm thick Ge layer deposited on the In-richest InGaAs buffer. The InGaAs and Ge layer patches are narrow, overall in the horizontal direction (0.15° for the plastically relaxed InGaAs thick buffer layer), sign of a good crystalline structure. The map around (004) direction provides the value of “c” lattice parameter parallel to the growth direction. Combining the (224) map with the one along (004) direction makes the measurement of the “a” lattice parameter, parallel to the surface, possible. The In concentration

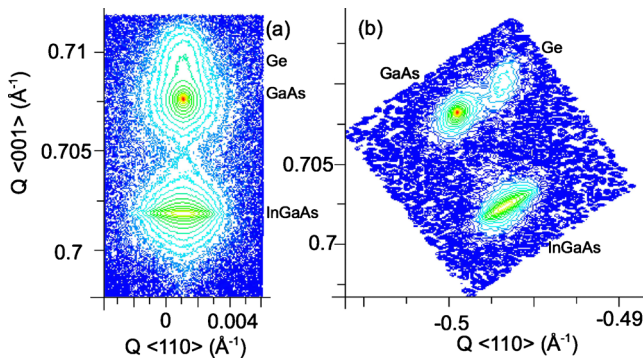


FIG. 2. (Color online) (a) 004 and (b) 224 HRXRD-RSM, collected along the same azimuthal direction. The RSMs are drawn in reciprocal space coordinates.

and strain relaxation ratio of the buffer were deduced from the lattice parameters and the elastic constants of InAs and GaAs references. For the three investigated samples, the InGaAs buffer layers were almost fully plastically relaxed (94% relaxation for the 4.8 and 8% In-rich buffers and $80 \pm 3\%$ relaxation for the 9.8% In-rich buffer). Due to the vicinity of the Ge and GaAs 004 diffraction spots, it was difficult to determine the Ge lattice parameters for the samples with low indium content. They were determined accurately only for the sample with the In-richest InGaAs buffer. The Ge and InGaAs in-plane “a” lattice parameters are equal indicating that the Ge layer is lattice matched with the InGaAs buffer. It confirms the good quality of the interface observed by TEM/STEM. Out-of-plane and in-plane lattice parameters are equivalent for the four $\langle 110 \rangle$ in-plane azimuthal directions. The deformation of tensile-strained germanium is thus purely tetragonal. For the sample grown on the 9.8% In-rich buffer, the parallel and vertical lattice parameters for tensile-strained germanium are 0.5685 nm and 0.5637 nm, respectively. These parameters are linked through the tetragonal strain relation $\varepsilon_{\perp} = -2(C_{12}/C_{11})\varepsilon_{\parallel}$, where $\varepsilon_{\perp} = [(a_{\perp} - a_0)/a_0]$, $\varepsilon_{\parallel} = [(a_{\parallel} - a_0)/a_0]$. Using a ratio $2(C_{12}/C_{11}) = 0.698$, one deduces a bulk germanium lattice constant of 0.56571 nm, in very close agreement with the published lattice constant value of germanium. The in-plane strain $\varepsilon_{\parallel} = \varepsilon_{xx} = \varepsilon_{yy}$ is 0.5% for this sample corresponding to a full strain transfer from InGaAs to Ge.

The strain state of the germanium layer was independently measured by Raman spectroscopy at 514 nm in backscattering geometry.^{12,15,18} The strain is deduced from the downshift in the Raman peak as compared to bulk germanium according to the relation $\Delta\omega = -415\varepsilon_{\parallel}$ (cm^{-1}) for a biaxial deformation.¹⁵ For the sample with a 9.8% indium content, a downshift of 2.3 ± 0.02 cm^{-1} was measured corresponding to an in-plane tensile strain of $0.554\% \pm 0.005\%$. The strain levels of the 4.8% and 8% In-content samples, 0.26% and 0.45%, respectively, were found to be lower, as expected, and independent of the Ge layer thickness (25 or 50 nm).

Figure 3 shows the room temperature photoluminescence spectra of *n*-doped tensile-strained germanium grown on different buffer layers. The spectra are measured with a PbS detector, thus, allowing to cover a large spectral range without detector cutoff. The indium contents of the buffer layers are indicated on the figure. The direct band gap radiative recombination of tensile-strained germanium is observed at room temperature, a feature not reported in previous studies of germanium on InGaAs buffers.^{15,18,19} This is particularly important as these layers are grown in order to achieve laser emission. The direct band gap dominates as the layer thickness is small and no significant reabsorption occurs. The photoluminescence shifts to longer wavelength as the tensile strain is increased. A shift of 103 nm as compared to relaxed germanium is observed for the sample with an 9.8% indium composition (top spectrum). The peak of the recombination of the strained layer is associated with the heavy hole band even if the light hole band is lower in energy for tensile-strained germanium, as shown in Ref. 13. Nonetheless, the recombination with the light hole band contributes to the broadening of the recombination as strain is increased. The in-plane tensile strain in the germanium layer can be deduced from the photoluminescence redshift according to the rela-

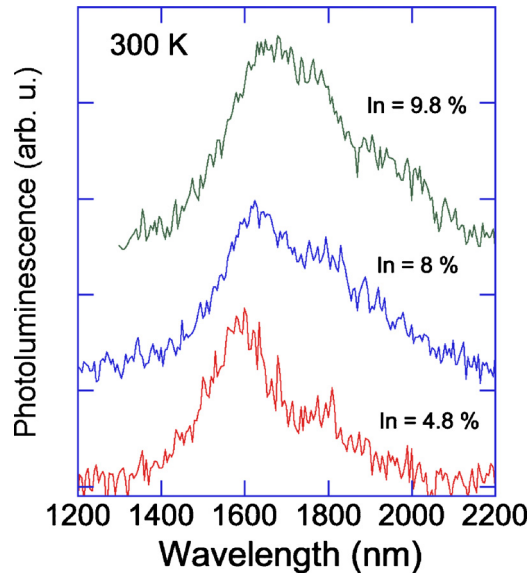


FIG. 3. (Color online) Room temperature photoluminescence spectra of three tensile-strained 50 nm thick germanium films for different indium content. The indium contents of the InGaAs buffer are indicated on the graph. The curves have been offset for clarity. The direct band gap recombination of relaxed germanium peaks at 1550 nm (not shown).

tion as obtained from a 30 band $\mathbf{k}\cdot\mathbf{p}$ formalism^{20,21} and the material deformation parameters $\Delta E_{\text{PL}} = -7.8 \times \varepsilon_{\parallel}$ (eV), where $\varepsilon_{\parallel} = \varepsilon_{xx} = \varepsilon_{yy}$ is the biaxial in-plane strain.^{13,22}

Figure 4 shows a comparison between the experimental in-plane strain values as a function of the in-plane lattice parameter of the buffer layer measured experimentally. A good agreement is obtained between the three methods. One can observe that at high indium content, the strain deduced from the photoluminescence measurement (0.64%) is slightly larger than the one deduced by Raman or XRD. An uncertainty exists for the exact position of the heavy hole photoluminescence maximum since the recombination is particularly broad. An 8 meV uncertainty on the photolumines-

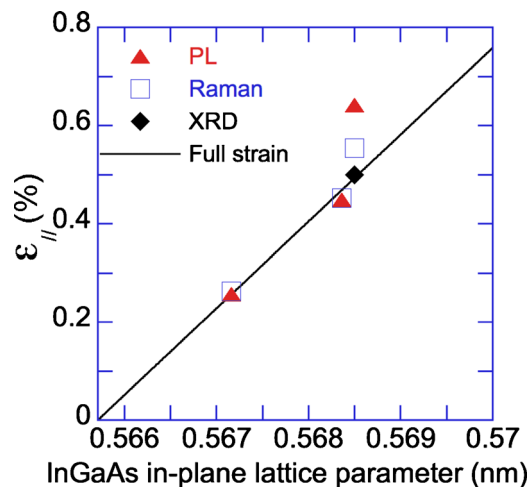


FIG. 4. (Color online) Measurement of the in-plane tensile strain of the Ge films as a function of the in-plane lattice parameter of the InGaAs buffer. The diamond corresponds to XRD, the squares to Raman measurements and the triangles to photoluminescence measurements. The full line corresponds to the expected full strain transfer from the InGaAs buffer to a coherently grown Ge layer.

cence maximum difference corresponds to an error bar of 0.1% for the biaxial strain. Sample inhomogeneities might contribute to the discrepancy. An uncertainty also exists on the values of deformation potentials for tensile-strained Ge.²² Finally, as the germanium layer is very thin and close to the surface, band bending, not considered in the calculation, might shift the recombination energy.

In conclusion, we have shown that high quality n -doped tensile-strained germanium layers can be obtained by metal-organic chemical vapor deposition on InGaAs buffers using IBGe as germanium precursor. These results open the route to the fabrication of highly-strained n -doped germanium layers which could exhibit net optical gains^{23,24} and potentially be embedded in resonators like photonic crystals.^{25,26}

¹J. Liu, X. Sun, R. Camacho-Aguilera, L. C. Kimerling, and J. Michel, *Opt. Lett.* **35**, 679 (2010).

²J. Liu, X. Sun, D. Pan, X. Wang, L. C. Kimerling, T. L. Koch, and J. Michel, *Opt. Express* **15**, 11272 (2007).

³S.-W. Chang and S. L. Chuang, *IEEE J. Quantum Electron.* **43**, 249 (2007).

⁴P. H. Lim, S. Park, Y. Ishikawa, and K. Wada, *Opt. Express* **17**, 16358 (2009).

⁵G. Pizzi, M. Virgilio, and G. Grosso, *Nanotechnology* **21**, 055202 (2010).

⁶M. El Kurdi, G. Fishman, S. Sauvage, and P. Boucaud, *J. Appl. Phys.* **107**, 013710 (2010).

⁷X. Sun, J. Liu, L. C. Kimerling, and J. Michel, *Appl. Phys. Lett.* **95**, 011911 (2009).

⁸M. El Kurdi, T. Kociniewski, T.-P. Ngo, J. Boulmer, D. Debarre, P. Boucaud, J. F. Damlencourt, O. Kermarrec, and D. Bensahel, *Appl. Phys. Lett.* **94**, 191107 (2009).

⁹Y. Ishikawa, K. Wada, D. D. Cannon, J. Liu, H.-C. Luan, and L. C. Kimerling, *Appl. Phys. Lett.* **82**, 2044 (2003).

¹⁰R. Soref, J. Kouvetakis, and J. Menendez, *Group IV semiconductor nanostructures*, MRS Symposia Proceedings No. 958 (Materials Research Society, Pittsburgh, 2007), p. 13.

¹¹J. Menéndez and J. Kouvetakis, *Appl. Phys. Lett.* **85**, 1175 (2004).

¹²Y.-Y. Fang, J. Tolle, R. Roucka, A. V. G. Chizmeshya, J. Kouvetakis, V. R. D'Costa, and J. Menendez, *Appl. Phys. Lett.* **90**, 061915 (2007).

¹³M. El Kurdi, H. Bertin, E. Martincic, M. de Kersauson, G. Fishman, S. Sauvage, A. Bosseboeuf, and P. Boucaud, *Appl. Phys. Lett.* **96**, 041909 (2010).

¹⁴T.-H. Cheng, K.-L. Peng, C.-Y. Ko, C.-Y. Chen, H.-S. Lan, Y.-R. Wu, C. W. Liu, and H.-H. Tseng, *Appl. Phys. Lett.* **96**, 211108 (2010).

¹⁵Y. Bai, K. E. Lee, C. Cheng, M. L. Lee, and E. A. Fitzgerald, *J. Appl. Phys.* **104**, 084518 (2008).

¹⁶E. Woelk, D. V. Shenai-Khatkate, R. L. DiCarlo, Jr., A. Amamchyan, M. B. Power, B. Lamare, G. Beaudoin, and I. Sagnes, *J. Cryst. Growth* **287**, 684 (2006).

¹⁷M. de Kersauson, R. Jakomin, M. El Kurdi, G. Beaudoin, N. Zerounian, F. Aniel, S. Sauvage, I. Sagnes, and P. Boucaud, *J. Appl. Phys.* **108**, 023105 (2010).

¹⁸Y. Hoshina, A. Yamada, and M. Konagai, *Jpn. J. Appl. Phys.* **48**, 111102 (2009).

¹⁹Y. Huo, H. Lin, R. Chen, M. Makarova, Y. Rong, M. Li, T. I. Kamins, J. Vuckovic, and J. S. Harris, *Appl. Phys. Lett.* **98**, 011111 (2011).

²⁰S. Richard, F. Aniel, and G. Fishman, *Phys. Rev. B* **70**, 235204 (2004).

²¹M. El Kurdi, S. Sauvage, G. Fishman, and P. Boucaud, *Phys. Rev. B* **73**, 195327 (2006).

²²J. Liu, D. D. Cannon, K. Wada, Y. Ishikawa, D. T. Danielson, S. Jongthammanurak, J. Michel, and L. C. Kimerling, *Phys. Rev. B* **70**, 155309 (2004).

²³J. Liu, X. Sun, L. C. Kimerling, and J. Michel, *Opt. Lett.* **34**, 1738 (2009).

²⁴C. Lange, N. S. Koster, S. Chatterjee, H. Sigg, D. Chrastina, G. Isella, H. von Kanel, M. Schafer, M. Kira, and S. W. Koch, *Phys. Rev. B* **79**, 201306 (2009).

²⁵M. El Kurdi, S. David, X. Checoury, G. Fishman, P. Boucaud, O. Kermarrec, D. Bensahel, and B. Ghyselen, *Opt. Commun.* **281**, 846 (2008).

²⁶T.-P. Ngo, M. El Kurdi, X. Checoury, P. Boucaud, J. F. Damlencourt, O. Kermarrec, and D. Bensahel, *Appl. Phys. Lett.* **93**, 241112 (2008).